View metadata, citation and similar papers at core.ac.uk

brought to you by CORE

provided by Missouri University of Science and Technology (Missouri S&T): Scholars' Mine

Missouri University of Science and Technology

Scholars' Mine

Electrical and Computer Engineering Faculty Research & Creative Works

Electrical and Computer Engineering

01 Jan 2005

Two Separate Continually Online-Trained Neurocontrollers for a Unified Power Flow Controller

Ganesh K. Venayagamoorthy
Missouri University of Science and Technology

Radha P. Kalyani

Follow this and additional works at: https://scholarsmine.mst.edu/ele_comeng_facwork

 Part of the Electrical and Computer Engineering Commons

Recommended Citation

G. K. Venayagamoorthy and R. P. Kalyani, "Two Separate Continually Online-Trained Neurocontrollers for a Unified Power Flow Controller," *IEEE Transactions on Industry Applications*, Institute of Electrical and Electronics Engineers (IEEE), Jan 2005.
The definitive version is available at https://doi.org/10.1109/TIA.2005.851571

This Article - Journal is brought to you for free and open access by Scholars' Mine. It has been accepted for inclusion in Electrical and Computer Engineering Faculty Research & Creative Works by an authorized administrator of Scholars' Mine. This work is protected by U. S. Copyright Law. Unauthorized use including reproduction for redistribution requires the permission of the copyright holder. For more information, please contact scholarsmine@mst.edu.

Two Separate Continually Online-Trained Neurocontrollers for a Unified Power Flow Controller

Ganesh K. Venayagamoorthy, *Senior Member, IEEE,* and Radha P. Kalyani, *Student Member, IEEE*

***Abstract*—The crucial factor affecting the modern power systems today is load flow control. The Unified Power Flow Controller (UPFC) provides an effective means for controlling the power flow and improving the transient stability in a power network. The UPFC has fast complex dynamics and its conventional control is based on a linearized model of the power system. This paper presents the design of neurocontrollers to provide better damping during transient and dynamic control. Two separate neurocontrollers are used for controlling the UPFC, one neurocontroller for the shunt inverter and the other for the series inverter. Simulation studies carried out in the PSCAD/EMTDC environment is described and results show the successful control of the UPFC and the power system with two neurocontrollers. Performances of the neurocontrollers are compared with the conventional proportional plus integral controllers for system oscillation damping under different operating conditions for large disturbances.**

***Index Terms*—Indirect adaptive control, neurocontrollers, neuroidentifiers, power system, Unified Power Flow Controller (UPFC).**

I. Introduction

With the ever-increasing complexities in power systems across the globe and the growing need to provide stable, secure, controlled, economic, and high-quality electric power—especially in today's deregulated environment—it is envisaged that flexible ac transmission system (FACTS) controllers are going to play a critical role in power transmission systems [1]. Transmission congestion results when there is insufficient capacity to transmit power over existing lines and maintain the required safety margins for reliability. FACTS enhance the stability of the power system both with its fast control characteristics and continuous compensating capability. The two main objectives of FACTS technology are to control power flow and increase the transmission capacity over an existing transmission corridor [2].

Gyugyi proposed the Unified Power Flow Controller (UPFC), a new generation of FACTS devices in 1991 [3]. The UPFC is a combination of a static synchronous compensator (STATCOM) and a static synchronous series compensator (SSSC) which are coupled via a common dc link, to allow bidirectional flow of real power between series output terminals of the SSSC and the shunt terminals of the STATCOM, and are controlled to provide concurrent real and reactive series line compensation without an external electric energy source. Practically, these two devices are two voltage-source inverters (VSIs), one connected in shunt with the transmission line through a coupling transformer and the other is inserted in series with the transmission line through an insertion transformer. The UPFC by means of angularly unconstrained series voltage injection is able to control, concurrently or selectively, the transmission line voltage, impedance, and angle or, alternatively, the real and reactive power flow in the line. The UPFC may also provide independently controllable shunt-reactive compensation.

Neural networks are suitable for multivariable applications since they can easily identify the interactions between the system's inputs and outputs. Their ability to learn and store information about system nonlinearities allows neural networks to be used for modeling and designing intelligent controllers for power systems [4], [5]. Thus, they offer alternatives for traditional linear and nonlinear control. A radial basis function (RBF) neural network controller for a UPFC based on the direct adaptive control scheme has been reported to improve the transient stability performance of a power system [6]. It is known that indirect adaptive control is able to control a nonlinear system with fast changing dynamics better, such as the power system. This is as a result of the dynamics being continually identified by a model. Advantages of the neurocontrollers over the conventional controllers are that they can adapt to the changes in system operating conditions automatically unlike the conventional controllers whose performances degrade for such changes and are required to be retuned to give the desired performance.

This paper presents the design of neurocontrollers (NCs) to control the UPFC and the power system in a single machine infinite bus power system setup. The design of a NC for only the series branch of UPFC has been proposed by the authors in [7]. The design of the series and shunt continually online trained (COT) NCs to replace the existing proportional plus integral (PI) controllers in the series and the shunt branches of a UPFC are based on the indirect adaptive control scheme. In addition, two other neural networks called neuroidentifiers (NIs) are designed to identify the hybrid complex nonlinear dynamics of the UPFC and the power system. The neurocontrollers are trained based

Paper MSDAD-05-09, presented at the 2003 Industry Applications Society Annual Meeting, Salt Lake City, UT, October 12–16, and approved for publication in the IEEE Transactions on Industry Applications by the Industrial Automation and Control Committee of the IEEE Industry Applications Society. Manuscript submitted for review October 15, 2003 and released for publication April 26, 2005. This work was supported by the University of Missouri Research Board and by the National Science Foundation under Grants ECS 0231632 and CAREER ECS 0348221.

The authors are with the Real-Time Power and Intelligent Systems Laboratory, University of Missouri, Rolla, MO 65409 USA (e-mail: gkumar@ieee.org; rpk5f9@umr.edu).

Digital Object Identifier 10.1109/TIA.2005.851571

0093-9994/$20.00 © 2005 IEEE

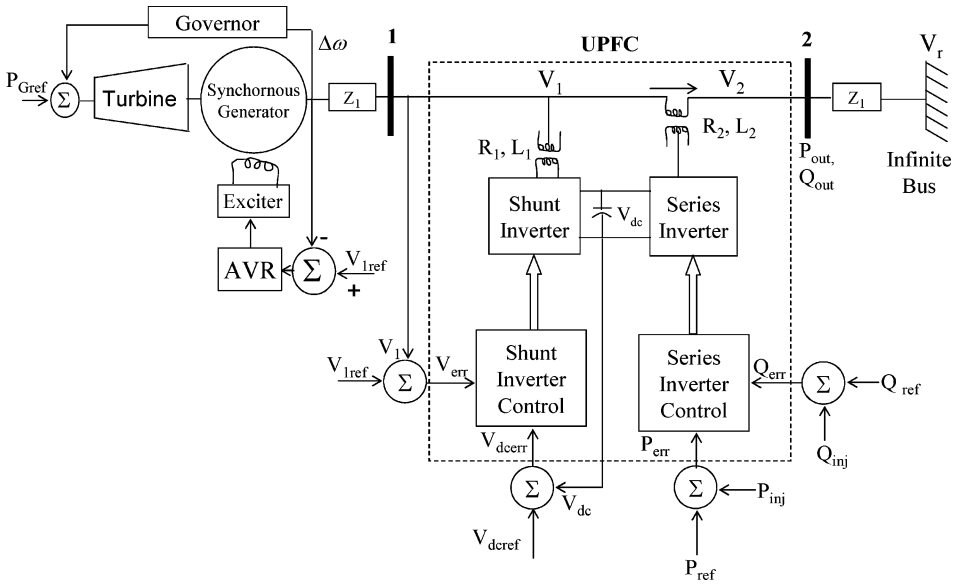

Fig. 1. SMIB system with the UPFC (the "*plant*").

on the dynamics modeled by the neuroidentifiers. In all, four COT neural networks are used for the complete UPFC control. A comparison of the performances of the neurocontrollers and PI controllers for damping system oscillations and voltage regulation are presented for a power system experiencing large disturbances at different operating points and conditions.

II. Power System With UPFC

For identifying and controlling the dynamics of a UPFC and a power system, the single-machine infinite-bus (SMIB) power system in Fig. 1 is simulated in a PSCAD/EMTDC environment. EMTDC is an electromagnetic transient simulator of electric networks with the capability of modeling complex power electronics, controls and the nonlinear power network [10]. PSCAD is the graphical user interface to EMTDC. The PSCAD/EMTDC combination is a powerful tool for visualizing the enormous complexity of portions of the electric power system [10].

The power system in Fig. 1 comprises a synchronous generator with exciter-automatic voltage regulator (AVR) and turbine-governor combinations connected to an infinite bus through two sections of transmission lines. The UPFC is placed between the two sections of the transmission lines, between bus 1 and 2 as shown in Fig. 1. This simple system is chosen in order to evaluate the performance of the UPFC with two different control strategies.

The series inverter provides the main function of the UPFC by injecting a voltage with magnitude V_2, which is controllable and a phase angle δ in series with the line via an insertion transformer. This injected voltage acts essentially as a synchronous ac voltage source. The transmission line current flows through this voltage source resulting in a reactive and active power exchange between itself and the ac system. The inverter generates the reactive power exchanged at the ac terminal internally. The active power exchanged at the ac terminal is converted into dc power, which appears at the dc link as a positive or negative real power.

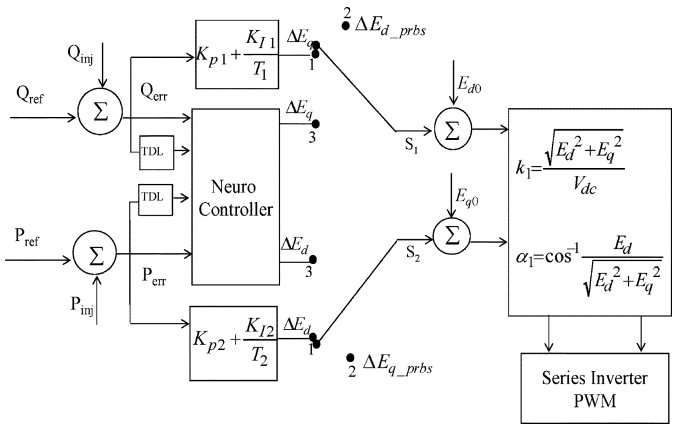

Fig. 2. Series inverter control with conventional PI controllers and neurocontroller.

The basic function of shunt inverter is to generate or absorb the real power demanded by series inverter at the common dc link. The power demand by the series inverter at the dc link is converted back to ac by the shunt inverter and fed to the transmission line bus via a shunt-connected transformer. In addition to this, the shunt inverter can also generate or absorb controllable reactive power if desired and thereby provides independent shunt reactive compensation for the line [11]–[14].

The three main control parameters of UPFC are voltage magnitude, voltage angle and shunt reactive current. Control of real and reactive power can be achieved by injecting series voltage with an appropriate magnitude and angle. The transient stability model for the shunt and series branch of a UPFC in the dq reference frame are given in the literature [8], [15]. The conventional shunt and series branch control of the UPFC is briefly described below.

A. Series Branch Control

The block diagram of the conventional PI controllers for series branch of the UPFC is shown in Fig. 2 (with the switches

S_1 and S_2 at position 1) [8], [15]. The control of series inverter can be achieved using PQ-decoupled control. The outputs of the control system are the modulation index k_1 and phase shift α_1. Neglecting the inverter losses, the injected active power P_{inj}, reactive power Q_{inj}, output active power P_{out}, and reactive power Q_{out} are given by

$$P_{\text{inj}} = \frac{V_2(E_q - E_q\cos\delta + E_d\sin\delta)}{X} \quad (1)$$

$$Q_{\text{inj}} = \frac{V_2E_d\cos\delta + V_2E_q\sin\delta - V_2E_d + E_d^2 + E_q^2}{X} \quad (2)$$

$$P_{\text{out}} = \frac{V_2^2\sin\delta + V_2E_q}{X} \quad (3)$$

$$Q_{\text{out}} = \frac{2V_2E_d\cos\delta + 2V_2E_q\sin\delta + E_d^2 + E_q^2}{2X} \quad (4)$$

where

$$V_2 = \sqrt{E_d^2 + E_q^2}$$
$$E_q = V_{\text{inj}}\sin(\theta_{\text{inj}})$$
$$E_d = V_{\text{inj}}\cos(\theta_{\text{inj}}). \quad (5)$$

It can be seen from (3) that P_{out} is mainly affected by E_q whereas (4) shows that Q_{out} is affected by both E_q and E_d. In incremental form, the line active and reactive power can be expressed in terms of ΔE_q and ΔE_d as given by (6a) and (6b).

$$\Delta P_{\text{out}} = \frac{V}{X}\Delta E_q \quad (6a)$$

$$\Delta Q_{\text{out}} = \frac{1}{X}(\Delta E_dV\cos\delta + \Delta E_qV\sin\delta + \Delta E_dE_{\text{do}} + \Delta E_qE_{\text{qo}}). \quad (6b)$$

However, it can be assumed in practice that $\cos\delta$ is close to unity and $\sin\delta$ is close to zero since the phase angle between the two buses (receiving and sending ends) on a transmission line is less than 30°, which leads to (7)

$$\Delta Q_{\text{out}} = \frac{1}{X}(V\Delta E_d + E_{\text{do}}\Delta E_d + E_{\text{qo}}\Delta E_q). \quad (7)$$

The NI is trained with switches S_1 and S_2 at position 2 and the NC controls the UPFC with switches S_1 and S_2 at position 3. The design of NI and NC are explained in Sections III and IV, respectively.

B. Shunt Branch Control

Control of the shunt active and reactive current is achieved by varying the shunt inverter voltage active E_{pd} and reactive components E_{pq}, respectively. The reactive power flow and shunt input voltage can be regulated by active voltage component E_{pd} and the dc-link capacitor voltage V_{dc} support can be achieved by regulating E_{pq}. Fig. 3 shows a typical block diagram of the conventional PI controllers for the UPFCs shunt branch control [8], [15]. The outputs of this control system are the modulation index k_2 and phase shift α_2. The PI controllers are replaced by the neurocontroller with switches S_1 and S_2 at position 3. The design procedure of the neuroidentifier and neurocontroller is explained in Sections III and IV, respectively.

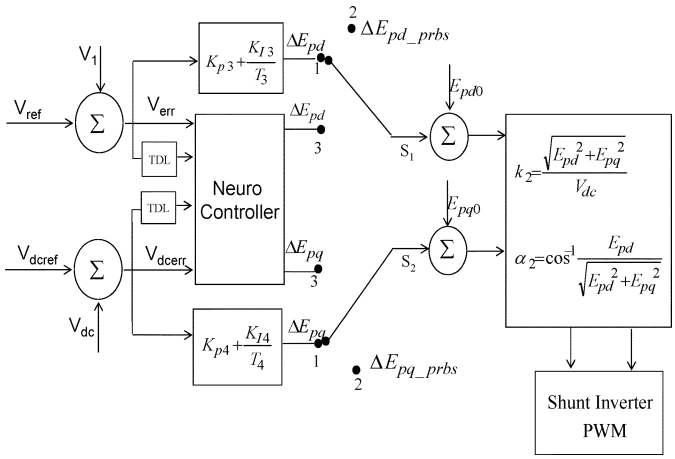

Fig. 3. Shunt inverter control with conventional PI controllers and neurocontroller.

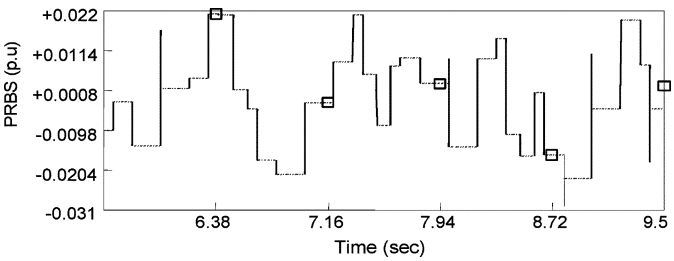

Fig. 4. E_{d_prbs} (one of the PRBS signals) applied to the series branch of UPFC with the switches S_1 and S_2 in position 2 in Fig. 2.

III. Design of Neuroidentifiers

Two neuroidentifiers, one for the series inverter and the other for the shunt inverter are used to identify the hybrid dynamics of the UPFC and the power system. These networks dynamically identify the controlling parameters of UPFC $\Delta E_{pd}, \Delta E_{pq}$, and $\Delta E_d, \Delta E_q$ which are the outputs of the controllers (Figs. 2 and 3). The NIs are developed using the series-parallel nonlinear autoregressive moving average (NARMA) model [4]. The two neuroidentifiers are continually online trained simultaneously to provide dynamic models at all times. The training of NIs takes place in two phases, namely, a *pre-control phase* and a *post-control phase* [5].

A. Pre-Control Phase

During this phase, the switches S_1 and S_2 in Figs. 2 and 3 are at position 2. The inputs to the NIs in this phase are the outputs from *plant* and the pseudorandom random binary signals (PRBS) in Figs. 4 and 5.

1) Series Neuroidentifier: The series UPFC branch neuoidentifier (SENI) in Fig. 6 is a three-layer feedforward neural network [also known as the multilayer perceptron (MLP)] with 13 inputs, a single hidden layer with 15 sigmoidal neurons, and two outputs. There are two different types of training that are carried out for SENI, namely, the forced training and the natural training.

During forced training, the dynamics of the plant are tracked by applying pertubations using PRBS which are fed to the plant

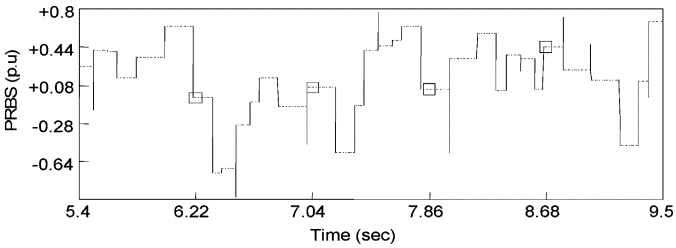

Fig. 5. E_{pd_prbs} (one of the PRBS signal) applied to the shunt branch of UPFC with the switches S_1 and S_2 in position 2 as shown in Fig. 3.

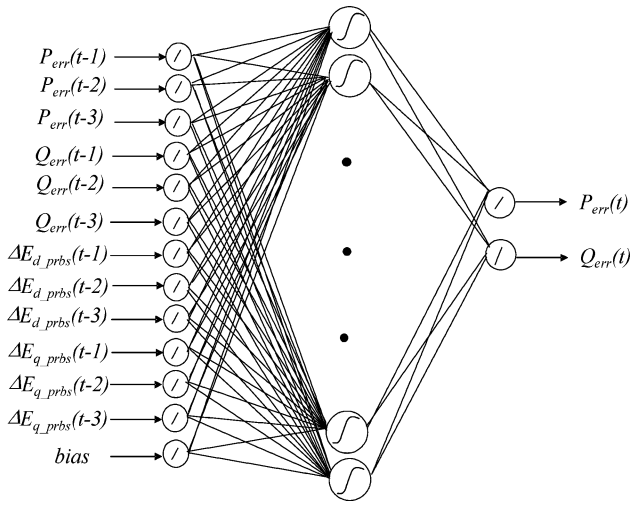

Fig. 6. Structure of neuroidentifier with 13 inputs, 15 sigmoidal neurons, and two outputs.

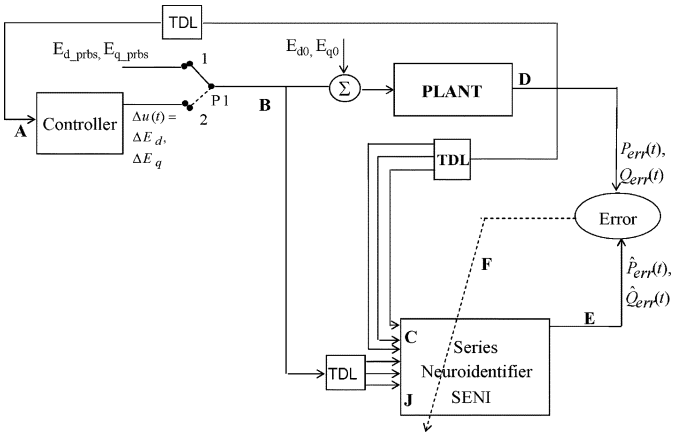

Fig. 7. Training of SENI to update the weights of the NI by backpropagating the error signals at $\mathbf{F}$.

at $\mathbf{B}$ in Fig. 7 by placing switch P1 at position 1. During natural training the inputs to the plant at $\mathbf{B}$ are the controller outputs, where the controller can be a conventional PI controller or a neurcontroller (switch P1 at 2). There are four different types of inputs, the first two types are the differences between the following signals: the measured real power and its reference value P_{err}, and, the measured reactive power and its reference value Q_{err}. The other two input types during forced training are the PRBS training signals—$\Delta E_{d\_\mathrm{prbs}}$ and $\Delta E_{q\_\mathrm{prbs}}$ (Fig. 4). In the pre-training phase, PRBSs are applied to excite all possible dynamics of the plant [4], [5]. These PRBS are fed to the series

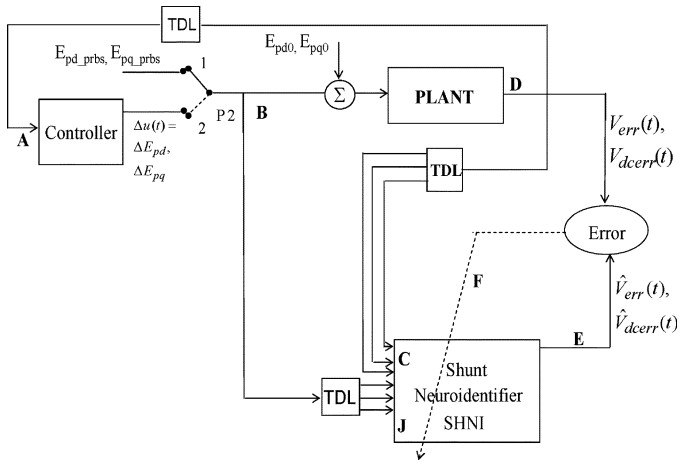

Fig. 8. Training of SHNI to update the weights of the NI by backpropagating the error signals at $\mathbf{F}$.

inverter at $\mathbf{B}$ and SENI at $\mathbf{C}$ with the switches S_1 and S_2 at position 2 (Fig. 2).

The typical PRBS signal applied is shown in Fig. 4. The frequency content of this signal is 1, 3, and 5 Hz. This is required to cause perturbation of all possible system dynamics so as to allow the SENI to learn better. All four different types of inputs are time delayed (TDL) by one sample period and together with their eight previously delayed values form the 12 inputs to the SENI. The outputs of the SENI in Fig. 7 at $\mathbf{E}$ are the estimated difference in the real power—$\hat{P}_{\mathrm{err}}$ and in the reactive power—$\hat{Q}_{\mathrm{err}}$ at the next time step. The outputs of SENI at $\mathbf{E}$ are compared to outputs of the plant at $\mathbf{D}$ and the error signals at $\mathbf{F}$ are used to update the weights of the SENI using the backpropagation (BP) algorithm. This process is repeated until a satisfactory error goal is obtained for the SENI training over a number of operating points of the plant.

2) Shunt Neuroidentifier: The shunt UPFC branch neuroidentifier (SHNI) is a three-layer feedforward neural network with 13 inputs, a single hidden layer with 18 sigmoidal neurons, and two outputs [similar to Fig. 6(a)]. As mentioned above for the SENI, the training of the SHNI is carried out in two phases—the forced and the natural training. There are four different types of inputs; the first two inputs to the NI are, namely, the deviation signals between the measured shunt voltage and its reference value V_{err}, the measured dc-link voltage and its reference V_{dcerr}, and the other two input types during forced training are the PRBS training signals $\Delta E_{pd\_\mathrm{prbs}}$ and $\Delta E_{pq\_\mathrm{prbs}}$ (swicth P2 at position 1 in Fig. 8) with magnitudes in proportion to the real and reactive components of shunt inverter voltage E_{pd} and E_{pq}, respectively.

All four types of inputs are time delayed by one sample period and together with their eight previously delayed values form the12 inputs to the SHNI at $\mathbf{C}$ (Fig. 8). The outputs of the SHNI at $\mathbf{E}$ are the shunt voltage deviation $\hat{V}_{\mathrm{err}}$ and dc-link voltage deviation $\hat{V}_{\mathrm{dcerr}}$ which are estimated one time step ahead. These PRBS signals are only fed to the shunt inverter at $\mathbf{C}$ and to the *plant* at $\mathbf{B}$ during the pre-training phase with the aid of switches S_1 and S_2 (Fig. 3). The outputs of SHNI in Fig. 8 at $\mathbf{E}$ are compared to outputs of the *plant* at $\mathbf{D}$ and the error signals at $\mathbf{F}$ are used to update the weights of the SHNI using the BP

algorithm. This process is repeated until a satisfactory error goal is obtained for the SENI training over a number of different possible operating points of the *plant*.

B. Post-Control Phase

During this phase, online training of the SENI and SHNI continue while the controllers (PI/NCs) are controlling their respective branches of the UPFC, with the switches S_1 and S_2 now at position 3 in Figs. 2 and 3. The design of the neurocontrollers is described in Section IV. The PRBS signals used in the pre-control phase are now set to zero and the outputs from the controllers are applied to the *plant*. The post-training steps for NIs (Figs. 7 and 8 with switches P1 and P2 at position 2) are described below.

1) The plant output signals at $\mathbf{D}$ are sampled and time delayed by one, two, and three sample periods.
2) The sampled signals from step 1) above are fed at $\mathbf{A}$ to the controllers which then calculates the control signals $\Delta E_{pd}, \Delta E_{pq}$, (SHNC) and $\Delta E_d, \Delta E_q$ (SENC) which are applied to control the *plant*.
3) These control signals are time delayed by one, two, and three sample periods, and, together with the signals from step 1) are fed to the NIs at $\mathbf{C}$.
4) The outputs at $\mathbf{D}$ ($P_{\rm err}(t), Q_{\rm err}(t)$ of series branch and $V_{\rm err}(t), V_{\rm dcerr}(t)$ of shunt branch) and the outputs of NIs at $\mathbf{E}$ ($\hat{P}_{\rm err}(t), \hat{Q}_{\rm err}(t)$ of SENI and $\hat{V}_{\rm err}(t), \hat{V}_{\rm dcerr}(t)$ of SHNI) are subtracted, respectively, to produce error signals at $\mathbf{F}$ which are backpropagated to update weights of the respective NIs.

IV. Design of Neurocontrollers

In the series and shunt UPFC branch neurocontroller design, each consists of two separate neural networks, one for the identifier/model (described in Section III) and other for the controller. The neurocontroller is used to replace the conventional PI controllers in each branch (Figs. 2 and 3). The training of neurocontrollers like the neuroidentifiers also takes place in two phases, namely, a *pre-control phase* and a *post-control phase* [5]. Both neurocontrollers are trained simultaneously.

A. Pre-Control Phase

During the pre-control phase the inputs to the NCs are the perturbated outputs from the *plant* as shown in Figs. 9 and 10. The PRBS signals (switches P3 and P4 at position 1) are applied as inputs to the NIs and to the *plant* to cause the necessary perturbations.

1) Series Neurocontroller: The series UPFC branch neurocontroller (SENC) in Fig. 9 is a three-layer feedforward neural network with six inputs, a single hidden layer with 18 sigmoidal neurons, and two outputs. There are two types of inputs to the SENC, namely, the $P_{\rm err}$ and the $Q_{\rm err}$. These signals at time $t-1, t-2$, and $t-3$ form the six inputs. The two outputs of SENC (ΔE_d and ΔE_q) are the control signals $\Delta u(t)$.

The outputs of the *plant* are fed into the desired response predictor (described in Section V), [4], which predicts $P_{\rm err}(t+1)$ and $Q_{\rm err}(t+1)$ at $\mathbf{K}$ (Fig. 10). The output of SENI at $\mathbf{E}$ is subtracted from the output of the desired response predictor at $\mathbf{K}$ to produce the error signal at $\mathbf{H}$ which is backpropagated through the SENI to obtain desired control signal $\Delta\hat{u}(t)$. The difference between $\Delta\hat{u}(t)$ and the outputs of SENC $\Delta u(t)$ generates the error signal at $\mathbf{L}$ which is used to update the weights of the SENC using BP. Pretraining is terminated when the weights of the SENC have converged for the PRBS signal applied over a number of operating points of the *plant*.

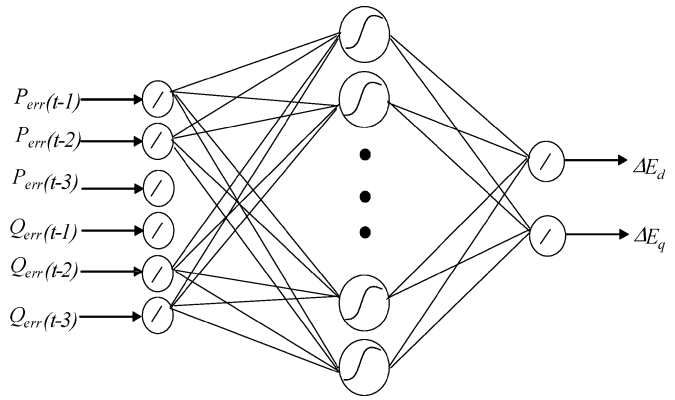

Fig. 9. Structure of neurocontroller with six inputs, 18 sigmoidal neurons, and two outputs.

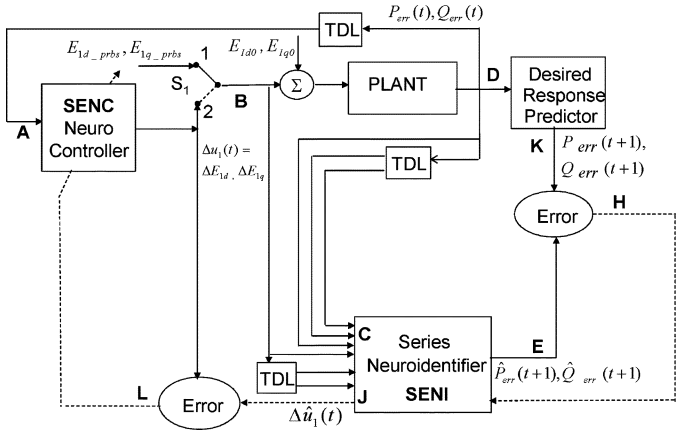

Fig. 10. Training of SENC to update the weights of the NC by backpropagating the error signals at $\mathbf{L}$.

2) Shunt Neurocontroller: The shunt UPFC branch neurocontroller (SHNC) in Fig. 11, is a three-layer feedforward neural network with six inputs, a single hidden layer with 18 sigmoidal neurons, and two outputs. Fig. 11 shows the SHNC development block diagram and, the respective inputs and outputs for the pretraining phase. The PRBS signals are applied to the input of the shunt UPFC branch and the SHNI by placing the switch P4 at position 1. The outputs of the plant are fed into the desired response predictor, which predicts $V_{\rm err}(t+1)$ and $V_{\rm dcerr}(t+1)$ at $\mathbf{K}$. The output of SHNI at $\mathbf{E}$ is subtracted from the output of the desired response predictor at $\mathbf{K}$ to produce the error signal at $\mathbf{H}$ which is backpropagated through the SHNI to obtain desired control signal $\Delta\hat{u}(t)$. The difference between $\Delta\hat{u}(t)$ and the outputs of SHNC generates the error signal at $\mathbf{L}$ which is used to update the weights of the SHNC using BP. Pre-training is terminated when the weights of the SHNI and SHNC have converged over a number of operating points.

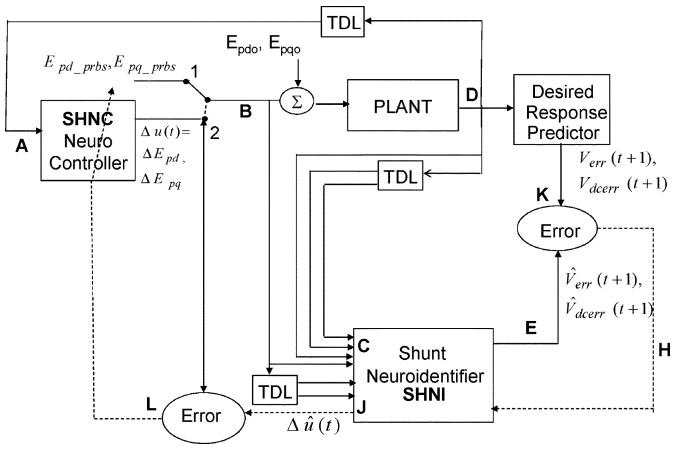

Fig. 11. Training of SHNC to update the weights of the NC by backpropagating the error signals at **L**.

The next phase of the training (post-control) for the NCs are carried out while the NCs are allowed to control the plant.

B. Post-Control Phase

During this phase, online training of the NCs continue while NCs are controlling their respective branches of the UPFC. The PRBS signals used in the pre-control phase are now set to zero and outputs from the NCs are applied to the *plant* (with switches P3 and P4 in Figs. 10 and 11 at position 2). The following steps are carried out during the post-control phase.

1) In the post-training of NCs, the output of the NIs at **E** ($\hat{P}_{\rm err}(t+1), \hat{Q}_{\rm err}(t+1)$ of SENI and $\hat{V}_{\rm err}(t+1), \hat{V}_{\rm dcerr}(t+1)$ of SHNI), and the desired response at **K** ($P_{\rm err}(t+1), Q_{\rm err}(t+1)$ of series branch and $V_{\rm err}(t+1), V_{\rm dcerr}(t+1)$ of shunt branch) are subtracted, respectively, to produce a second set of error signals at **H**. The error signals at **H** are backpropagated through the NIs and their derivatives are obtained at **J** (with the weights of NIs fixed). The backpropagated signals at **J** are subtracted from the output signals of the NCs to produce other error signals at **L**.
2) These error signals at **L** are then used to update the weights of the NCs using the BP algorithm. This causes the NCs to change its output in a way driving the error signals at **L** to zero.
3) New control signals are calculated $\Delta E_{pd}, \Delta E_{pq}$ for the shunt branch and $\Delta E_d, \Delta E_q$ for the series branch using the updated weights in step 2) and are then applied at next time step $(t+1)$ to the *plant* at **B**.
4) These steps are repeated for the subsequent time periods [4].

V. Desired Response Predictor

The desired response predictor (DRP) in Figs. 10 and 11 is designed [17] to have the following characteristics.

1) It must be flexible enough to modify the dynamic performance of the neurocontroller such as the rise time and damping.
2) The desired response signal must ensure that the UPFC is inherently stable at all times. In other words, the predictor must be stable.
3) The desired response signal must incorporate the effects of a damping controller for the plant.

The DRP is designed on the basis of guiding the disturbed output variables $X(k)$ to a desired steady operating point or set point, in a step-by-step fashion. In other words, a desired trace of outputs from k to $k+1$ can be predicted, based on the present and past-time values of the outputs. The equation of the DRP is given in (8)

$$\hat{X}(k+1) = A_0 X(k) + A_1 X(k-1) + \cdots + A_N X(k-N). \quad (8)$$

$A_i (i = 0, 1, \ldots, \mathrm{N})$ are chosen so that any disturbed output variable always transfers toward the desired steady operating point, that is the DRP is always globally asymptotically stable. $\hat{X}$ is the value predicted for the next immediate time step and X for example in the case of the shunt branch of the UPFC can be the voltage deviations ΔV at the bus where the shunt inverter is connected or its dc capacitor voltage deviations.

In (8), it is assumed that each output variable X of the DRP is a linear combination of the independently predicted output variables of the dynamic system. The magnitude of the coefficients, A_i, determine the magnitude of the error signal between the neuroidentifier output and the desired response signal (or predictor) $\hat{X}$, and therefore, the magnitude of the error to be backpropagated to the neurocontroller to adapt its weights.

If the output $X(k)$ is bounded for $0 < k < \infty$ and

$$\mathrm{Lim}\_k \to \infty (X(k) - \hat{X}(k)) = 0 \quad (9)$$

then a predictor can be designed which forces the UPFC device to respond, by means of the neurocontroller, to return the system to its desired setpoints [17]. The magnitude of the forcing signal depends on the coefficients A_i.

If (9) does not hold then the control variables will not return the system to its setpoints after a disturbance. The fundamental assumption made in this design is that it is possible for a controller to return system variables to its set points after a disturbance as explained in [4] and [17].

The desired response predictor used for training SENC is given by (10) and (11). Similarly the desired response predictor for training SHNC is given by (12) and (13)

$$P_{\rm err}(t+1) = P_{\rm err}(t) + P_{\rm err}(t-1) + P_{\rm err}(t-2) \quad (10)$$

$$Q_{\rm err}(t+1) = 0.1Q_{\rm err}(t) + 0.1Q_{\rm err}(t-1) + 0.4Q_{\rm err}(t-2) \quad (11)$$

$$V_{\rm err}(t+1) = 0.1V_{\rm err}(t) + 0.1V_{\rm err}(t-1) + 0.1V_{\rm err}(t-2) \quad (12)$$

$$V_{\rm dcerr}(t+1) = V_{\rm dcerr}(t) + V_{\rm dcerr}(t-1) + V_{\rm dcerr}(t-2). \quad (13)$$

The next section describes the simulation results of the power system with single and double transmission lines.

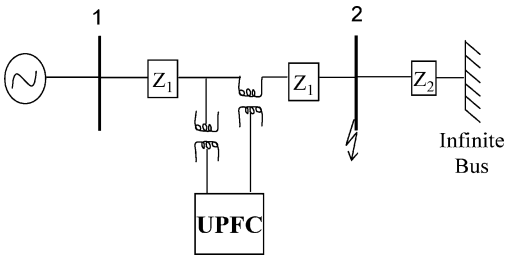

Fig. 12. SMIB with a single transmission line and a UPFC.

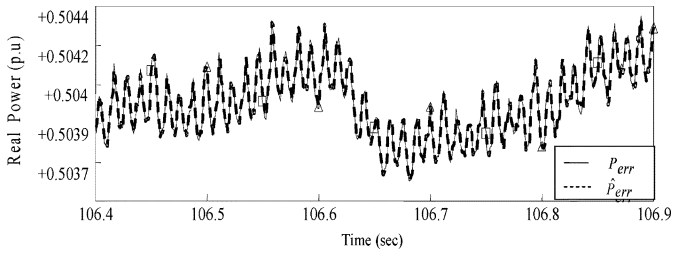

Fig. 13. Actual signal $P_{\rm err}$ of the plant and estimated signal $\hat{P}_{\rm err}$ by the SENI..

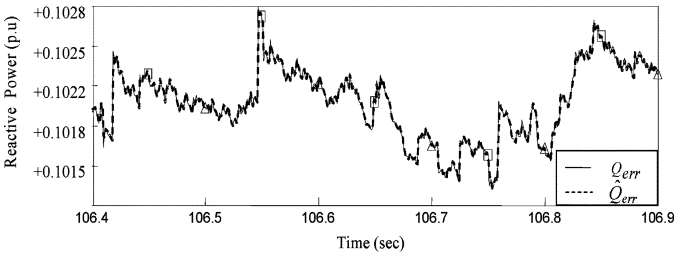

Fig. 14. Actual signal $Q_{\rm err}$ of the plant and estimated signal $\hat{Q}_{\rm err}$ by the SENI..

VI. Simulation Results

A. SMIB With Single Transmission Line

The system model in Fig. 12 comprises a synchronous generator (590 MVA, 38 kV line to line) [9] operating at real power, $P = 0.5$ p.u and reactive power, $Q = 0.1$ p.u, with a single transmission line. The governor and turbine models are the IEEE standard models of PSCAD/EMTDC [10]. The parameters of PI controllers are fine tuned for this operating point using the time response analysis [16]. A sampling frequency of 10 kHz is used to sample the outputs of the *plant*.

1) Neuroidentification of Plant Dynamics: Identification of the error signals $P_{\rm err}(t), Q_{\rm err}(t)$ by SENI and $V_{\rm err}(t), V_{\rm dcerr}(t)$ by SHNI are carried out at different operating points and their weights are continually updated. The training signals fed to NIs—$\Delta E_{d\_{\rm prbs}}, \Delta E_{q\_{\rm prbs}}$, and $\Delta E_{pd\_{\rm prbs}}, \Delta E_{pq\_{\rm prbs}}$ are like those shown in Figs. 4 and 5. Figs. 13 and 14 show the outputs of SENI $(\hat{P}_{\rm err}(t), \hat{Q}_{\rm err}(t))$ and, Figs. 15 and 16 show the outputs of SHNI $(\hat{V}_{\rm err}(t), \hat{V}_{\rm dcerr}(t))$. It is observed from the plots that the series identifiers reach an error goal of 0.000 01 p.u in 100 s of simulation while the shunt identifiers reach an error goal of 0.001 p.u in the same time during the training in the pre-control phase. This convergence is sufficient for the NC design.

2) Neurocontrol of Plant: The SENC and SHNC attain error goals in similar time periods comparably to the SENI and SHNI,

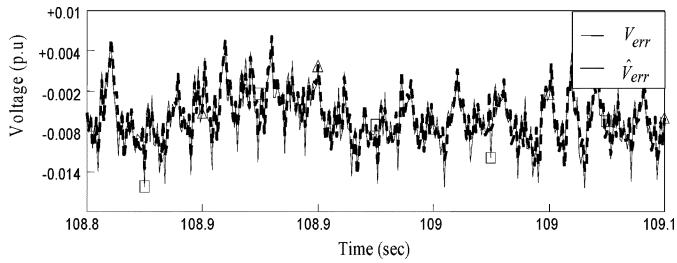

Fig. 15. Actual signal $V_{\rm err}$ of the plant and estimated signal $\hat{V}_{\rm err}$ by the SHNI.

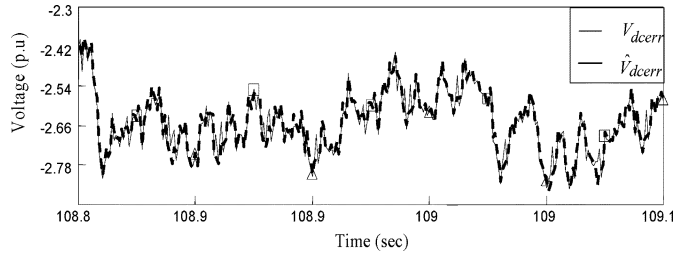

Fig. 16. Actual signal $V_{\rm dcerr}$ of the plant and estimated signal $\hat{V}_{\rm dcerr}$ by the SHNI.

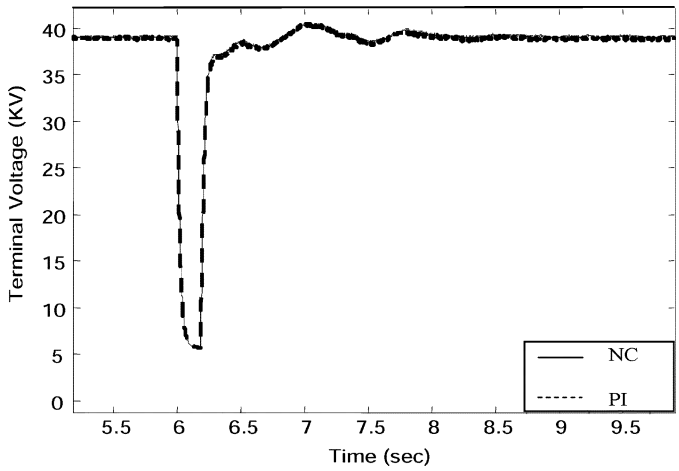

Fig. 17. Terminal voltage response of the synchronous generator operating ($P = 0.5$ p.u and $Q = 0.1$ p.u) for a 180-ms three-phase short circuit at bus 2.

respectively, during the pre-control training phase. The NCs and the PI controllers' performances are evaluated by applying a 180-ms three-phase short-circuit fault at bus 2 at three different operating points given below. The figures below show the response of the *plant* with the NCs (SENC and SHNC) in solid lines and with the PI controllers in dashed lines.

a) First Operating Point—$P = 0.5$ p.u and $Q = 0.1$ p.u: Figs. 17 and 18 show the terminal voltage and speed responses, respectivel, for the two controllers (NCs and PIs). It can be observed from these figures that the performances of both controllers are similar at this operating point. The rise time and settling times of the responses with the PI controllers and neurocontrollers are the same. This is because the PI controllers are fine tuned initially for this operating point.

b) Second Operating Point—$P = 0.65$ p.u and $Q = 0.12$ p.u: Figs. 19 and 20 show the terminal voltage and load angle responses, respectively. For this operating point, it can be seen that the responses with the NCs are better than that with the PI

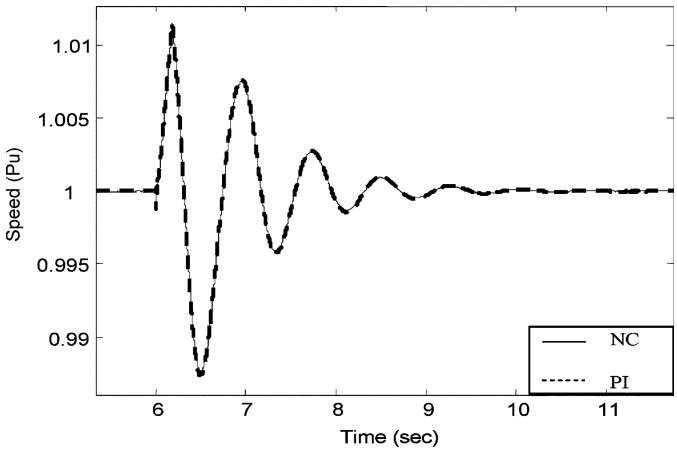

Fig. 18. Speed response of the synchronous generator operating ($P = 0.5$ p.u and $Q = 0.1$ p.u) for a 180-ms three-phase short circuit at bus 2.

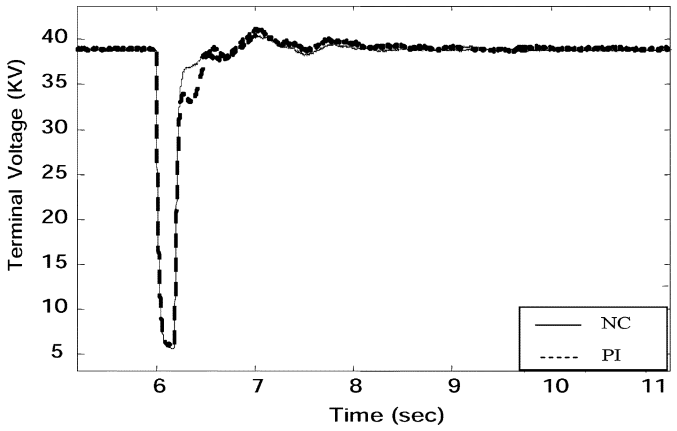

Fig. 19. Terminal voltage response of the synchronous generator operating ($P = 0.65$ p.u and $Q = 0.12$ p.u) for a 180–ms three-phase short circuit at bus 2.

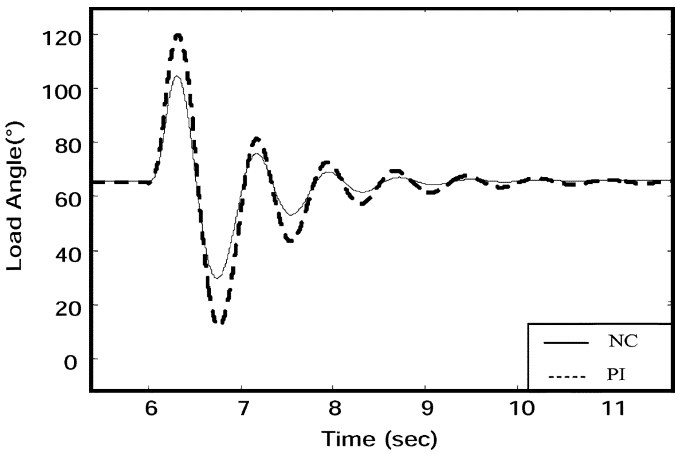

Fig. 20. Load angle response of the synchronous generator operating ($P = 0.65$ p.u and $Q = 0.12$ p.u) for a 180-ms three-phase short circuit at bus 2.

controllers for damping the system oscillations. It can be observed especially from Fig. 20 that the PI controllers' performances have degraded. The maximum overshoot with the PI controllers is about 20% more than seen with the neurocontrollers and settling time with PI controllers is about 60% longer than that with neurocontrollers.

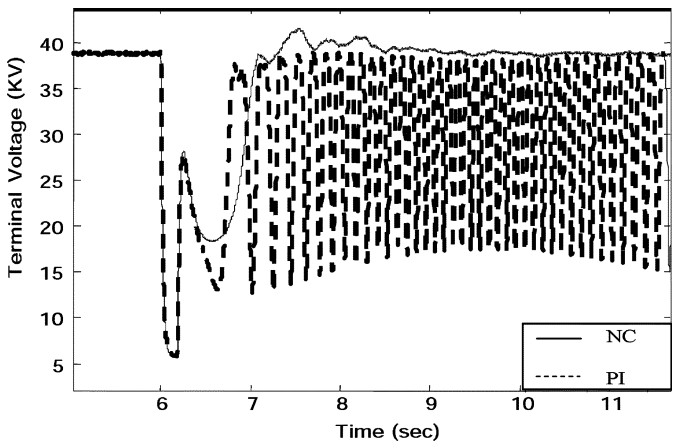

Fig. 21. Terminal voltage response of the synchronous generator operating ($P = 0.8$ p.u and $Q = 0.15$ p.u) for a 180-ms three-phase short circuit at bus 2.

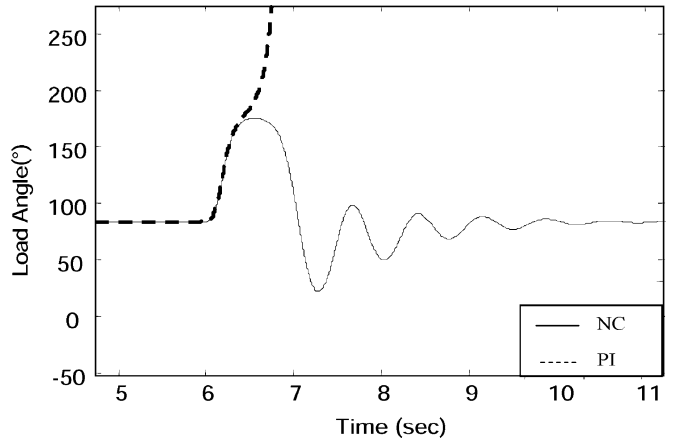

Fig. 22. Load angle response of the synchronous generator operating ($P = 0.8$ p.u and $Q = 0.15$ p.u) for a 180-ms three-phase short circuit at bus 2.

c) Third Operating Point—$P = 0.8$ p.u and $Q = 0.15$ p.u: Figs. 21 and 22 show the terminal voltage and load angle responses, respectively, for this operating point which is much further away from the one at which the PI controllers are fine tuned. It can be clearly seen from these figures that the *plant* with PI controllers have sustained oscillations in the terminal voltage and the load angle increases drastically after the fault, loosing stability. The *plant* with NCs on the other hand damps out the oscillations and restores the system to stability. The NCs give performances similar to those at previous operating points and maintains *plant* stability. This is because NCs are trained online and hence they are able to adapt to changes in operating conditions with the aid of the neuroidentifiers.

B. SMIB With Double Transmission Line

The system model in Fig. 23 is the same power system as that in Fig. 12 except that the single transmission line is replaced by a double transmission line. The UPFC is installed on transmission line 1 between buses 4 and 5. A load of $P = 0.25$ p.u and $Q = 0.1$ p.u is added at bus 3. The NC and the PI controllers' performances are evaluated by applying three phase short circuit fault of different durations for the synchronous generator operating point at $P = 0.8$ p.u and $Q = 0.2$ p.u.

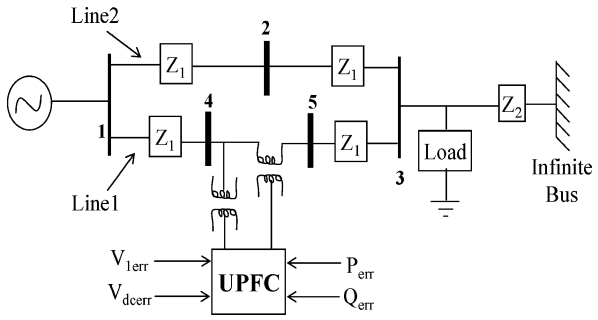

Fig. 23. SMIB built with two transmission lines, the UPFC on Line1, and a load at bus 3.

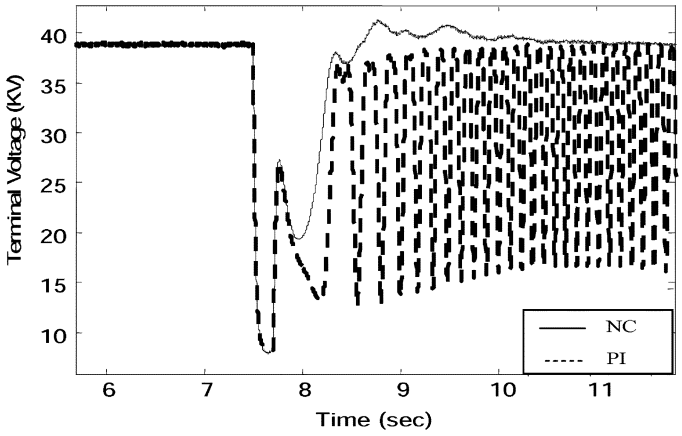

Fig. 24. Terminal voltage response of the synchronous generator ($P = 0.8$ p.u and $Q = 0.2$ p.u) for a 200-ms three-phase short circuit at bus 3 (Fig. 23).

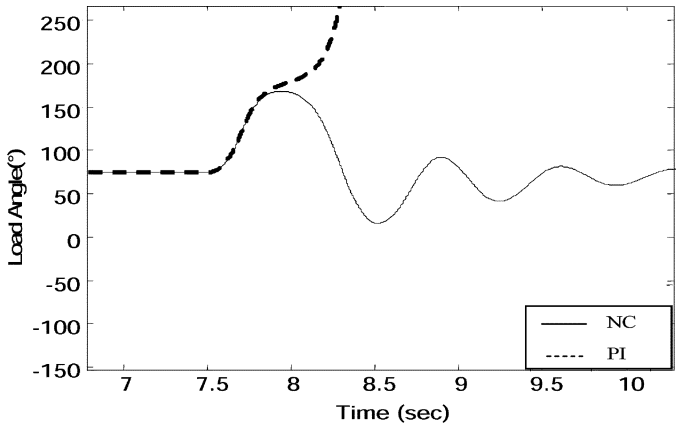

Fig. 25. Load angle response of the synchronous generator ($P = 0.8$ p.u and $Q = 0.2$ p.u) for a 200-ms three-phase short circuit at bus 3 (Fig. 23).

1) Three Phase Fault for 200 ms Duration: A three-phase fault of duration 200 ms is applied at bus 3 (Fig. 23) at time $t = 7.5$ s. The effective control of the UPFC by SENC and SHNC can be seen from the responses of terminal voltage and load angle in Figs. 24 and 25, respectively. It is seen that at this operating point for this fault, the conventional PI controllers completely fail and the *plant* goes unstable. The *plant* with the NCs survive through the fault and returns to stability smoothly in about 3 s.

2) Three Phase Fault for 305 ms Duration: A three-phase fault of duration 305 ms is applied at bus 2 and at time $t = 7.5$ s. The terminal voltage and load angle responses are shown in Figs. 26 and 27, respectively. It is observed that at this operating point for this fault along one of the double transmission lines, the conventional PI controllers completely fail and the *plant* goes unstable, whereas the *plant* with the NCs survive through the 305-ms fault and returns to stability smoothly in about 4 s.

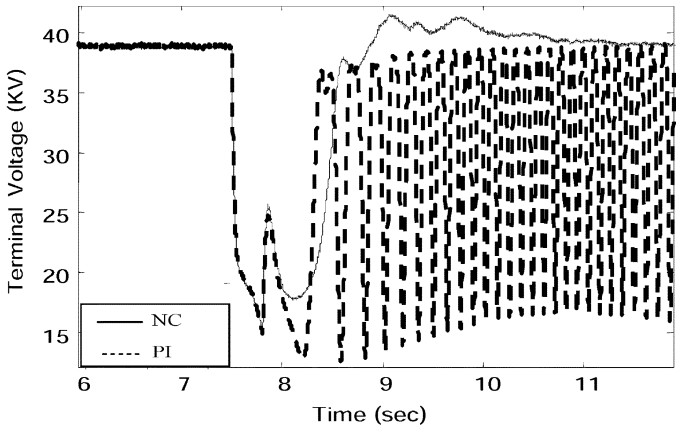

Fig. 26. Terminal voltage response of the synchronous generator ($P = 0.8$ p.u and $Q = 0.2$ p.u) for a 305-ms three-phase short circuit at bus 2 (Fig. 23).

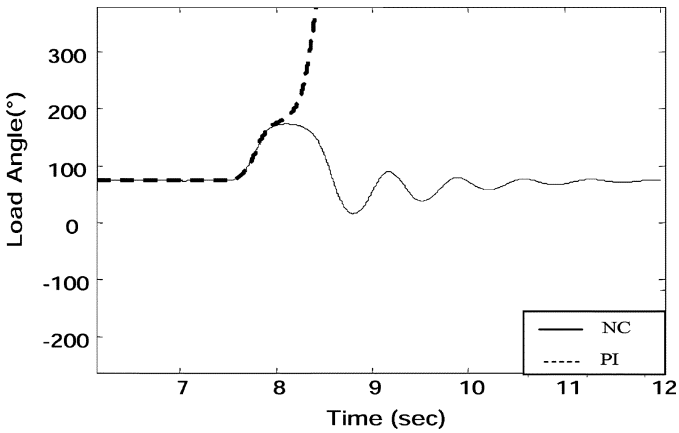

Fig. 27. Load angle response of the synchronous generator ($P = 0.8$ p.u and $Q = 0.2$ p.u) for a 305-ms three-phase short circuit at bus 2 (Fig. 23).

3) Double Three-Phase Short Circuits: Two three-phase faults are applied to the *plant*, first one of duration 200 ms on bus 3 (Fig. 23) applied at $t = 7.5$ s and then a second one of duration 105 ms is applied at $t = 9.5$ s on bus 2. Terminal voltage and load angle responses are shown in Figs. 28 and 29, respectively.

The *plant* is found to be stable after these double faults with the NCs unlike the case with the PI controllers. It is also observed that in all the tests above, the dc voltage excursions are rapidly damped out and this is essential for the successful operation of the series and shunt inverters of the UPFC. The system was not tested for PI controllers because of its failure in the previous test.

VII. Conclusion

In this paper, the design of two continually online trained neurocontrollers to provide adaptive nonlinear control of the

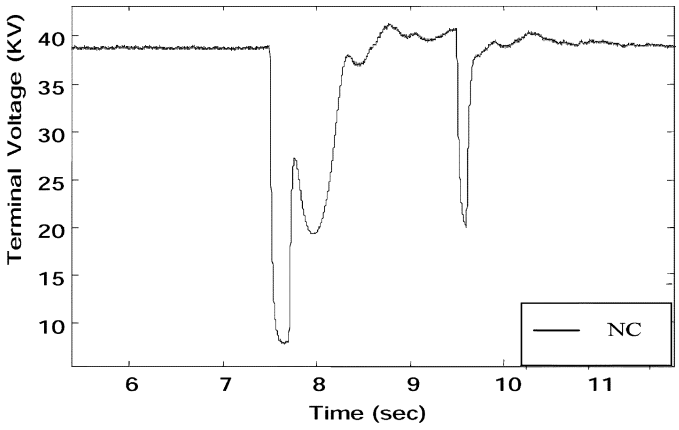

Fig. 28. Terminal voltage response of the synchronous generator ($P = 0.8$ p.u and $Q = 0.2$ p.u) for two three-phase faults, one for 200 ms at bus 3 applied at $t = 7.5$ s and another for 105-ms at bus 2 applied at $t = 9.5$ s (Fig. 23).

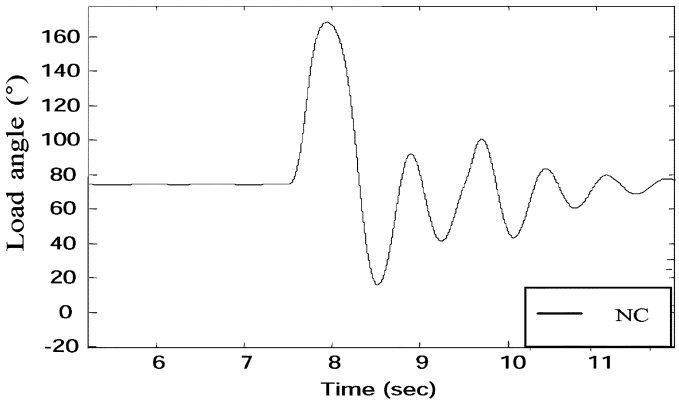

Fig. 29. Load angle response of the synchronous generator ($P = 0.8$ p.u and $Q = 0.2$ p.u) for two three-phase faults, one for 200 ms at bus 3 applied at $t = 7.5$ s and another for 105 ms at bus 2 applied at $t = 9.5$ s (Fig. 23).

series and shunt UPFC inverters over a wide range of operating conditions was presented. It has been shown that two separate neural networks are able to identify successfully the hybrid complex dynamics of a unified power flow controller and the power system; and another two separate neural networks are able to control the UPFC better than the conventional PI controllers. A superior performance of the neurocontrollers over the conventional controllers can be observed as a result of the online training of the neuroidentifiers and neurocontrollers which *never* stops. The initial promising results of the neurocontrollers imply that the electric power system equipped with such intelligent controllers can survive small and large disturbances thus preventing the power system from brownouts and blackouts. Future work involves extending the control strategy to a large power system with multiple FACTS devices. Identifying and mitigating the dynamics that may result from FACTS device interactions will become necessary.

APPENDIX

The power system used here comprises a synchronous generator whose parameters given in Table I are obtained from [9]. The ratings of the generator are as follows:

rated power—590 MVA;
rated voltage—22 kV;

TABLE I
GENERATOR PARAMETERS.

T_{d0}' = 4.2 s	X_d' = 0.28 p.u
T_{d0}" = 32 ms	X_d" = 0.215 p.u
T_{q0}" = 0.062 s	X_q = 2.02 p.u
X_d = 2.11 p.u	X_q" = 0.215 p.u

rated current—8.39 kA;
inertia, H—3.5 s.

The transmission line parameters are: $Z_1 = 0.01 + j0.2$ and $Z_2 = 0.005 + j0.05$.

The *exciter model* is the standard IEEE model of PSCAD [10] and its parameters are as follows:

lead time constant—0.0 s;
lag time constant—0.0 s;
regulator gain—400 p.u;
regulator time constant—0.02 s;
maximum regulator internal voltage (V_{AMAX})—20;
minimum regulator internal voltage (V_{AMIN})—20;
maximum regulator output (V_{RMAX})—10 p.u.;
maximum regulator output (V_{RMIN})—10 p.u.;
rated feedback gain (K_F)—0.03 p.u.;
rated feedback time constant (T_F)—1 s
exciter time constant (T_E)—0.8 s;
exciter constant related to field (K_E)—1.00 p.u.;
field circuit commutating reactance (K_C)—0.2 p.u,;
demagnetizing factor—(K_D)—0.38 p.u.;
saturation at VE1—0.1 p.u.;
exciter voltage for SE1—4.18 p.u.;
saturation at VE2—0.03 p.u.;
exciter voltage for SE2—3.14 p.u.

The turbine and governor models are also standard IEEE models available in PSCAD [10] and their parameters are given below.

For turbine:

head at rated conditions—1 p.u.;
output power at rated conditions—1 p.u.;
gate position at rated conditions—1 p.u.;
no-load water flow at rated head—0.05 p.u.;
initial operating head—1 p.u.;
water starting time (T_W)—2 s;
penstock head loss coefficient (D)—0.02 p.u.;
turbine damping constant (D)—0.5.

For governor:

speed reference—1 p.u.;
dead-band value—0;
permanent droop (R_p)—0.04 p.u.;
maximum gate position—1 p.u.;
minimum gate position—0 p.u.;
maximum gate opening rate—0.16 p.u./s;
maximum closing rate—0.16 p.u./s;
servo motor time constant—0.05 s;
servo gain—5 p.u.;
main servo time constant—0.2 s;
temporary droop—0.4 p.u.;

dashpot time constant—5 s.

The parameters of the UPFC PI controllers which are obtained by time response analysis are given below.

UPFC ratings:

series branch—185 MVA;
shunt branch—30 MVA;
series transformer ratings—22 kV/180 kV and 185 MVA;
shunt transformer ratings—38.10/1 kV and 30 MVA;
V_{dcbase}—6 kV;
C—9000 μF.

For shunt branch:

K_{p1}—1.2;
K_{I1}—0.05;
K_{p2}—0.5;
K_{I2}—0.05.

For series branch:

K_{p1}—3.5;
K_{I1}—0.1;
K_{p2}—3.5;
K_{I2}—0.1.

REFERENCES

[1] R. M. Mathur and R. K. Varma, *Thyristor-Based Facts Controllers for Electrical Transmission Systems*. New York: IEEE Press/Wiley, 2002.

[2] L. Chunlei, S. Hongbo, and D. C. Yu, "A novel method of power flow analysis with unified power flow controller (UPFC)," in *Proc. IEEE-PES Winter Meeting*, vol. 4, 2000, pp. 2800–2805.

[3] N. G. Hingorani and L. Gyugyi, *Understanding FACTS Concepts and Technology of Flexible AC Transmission Systems*. New York: IEEE Press, 2000.

[4] G. K. Venayagamoorthy and R. G. Harley, "Two separate continually online-trained neurocontrollers for excitation and turbine control of a turbo generator," *IEEE Trans. Ind. Appl.*, vol. 38, no. 3, pp. 887–893, May/Jun. 2002.

[5] ——, "A continually online trained neurocontroller for excitation and turbine control of a turbo generator," *IEEE Trans. Energy Convers.*, vol. 16, no. 3, pp. 261–269, Sep. 2001.

[6] P. K. Dash, S. Mishra, and G. Panda, "A radial basis function neural network controller for UPFC," *IEEE Trans. Power Syst.*, vol. 15, no. 4, pp. 1293–-1299, Nov. 2000.

[7] R. P. Kalyani and G. K. Venayagamoorthy, "A continually online trained neurocontroller for the series branch control of the UPFC," in *Proc. INNS-IEEE Int. Joint Conf. Neural Networks*, vol. 4, Jul. 2003, pp. 2982–2987.

[8] L. Y. Dong, L. Zhang, and M. L. Crow, "A new control strategy for the unified power flow controller," in *Proc. IEEE-PES Winter Meeting*, vol. 1, 2002, pp. 562–566.

[9] P. M. Anderson and A. A. Fouad, *Power System Control and Stability*. New York: IEEE Press, 1994.

[10] *PSCAD/EMTDC User's Guide, version 3.0*, Manitoba HVDC Research Centre Inc., Winnipeg, MB, Canada, 1998.

[11] B. A. Renz, A. Keri, A. S. Mehraban, C. Schauder, E. Stacey, L. Kovalsky, L. Gyugyi, and A. Edris, "AEP unified power flow controller performance," *IEEE Trans. Power Del.*, vol. 14, no. 4, pp. 1374–1381, Oct. 1999.

[12] A. Edris, "FACTS technology development: An update," *IEEE Power Eng. Rev.*, vol. 20, no. 3, pp. 4–9, Mar. 2000.

[13] S. Wei and X. Zheng, "Per unit model of UPFC and its optimal control," in *Proc. IEEE-PES Winter Meeting*, vol. 3, 2000, pp. 1105–1108.

[14] T. T. Ma and K. L. Lo, "Nonlinear power system damping control strategies for the unified power flow controller (UPFC)," in *Proc. PowerCon'00*, vol. 2, 2000, pp. 673–678.

[15] L. Dong, M. L. Crow, Z. Yang, C. Shen, L. Zhang, and S. Atcitty, "A reconfigurable FACTS system for university laboratories," *IEEE Trans. Power Syst.*, vol. 19, no. 1, pp. 120–128, Feb. 2004.

[16] K. Ogata, *Modern Control Engineering*, 3rd ed. Upper Saddle River, NJ: Prentice-Hall, 1996.

[17] G. K. Venayagamoorthy, R. G. Harley, and D. C. Wunsch, "Dual heuristic programming excitation neurocontrol for generators in a multimachine power system," *IEEE Trans. Ind. Appl.*, vol. 39, no. 2, pp. 382–394, Mar./Apr. 2003.

Ganesh Kumar Venayagamoorthy (M'97–SM'02) received the B.Eng. (Honors) degree with first class honors in electrical and electronics engineering from the Abubakar Tafawa Balewa University, Bauchi, Nigeria, in 1994, and the M.Sc.Eng. and Ph.D. degrees in electrical engineering from the University of Natal, Durban, South Africa, in 1999 and 2002, respectively.

He was a Senior Lecturer at the Durban Institute of Technology, South Africa, prior to joining the University of Missouri, Rolla (UMR), as an Assistant Professor in the Department of Electrical and Computer Engineering in May 2002. He directs the Real-Time Power and Intelligent Systems Laboratory at UMR. His research interests are in computational intelligence, power systems, evolvable hardware, and signal processing. He has published over 120 papers in refereed journals and international conference proceedings.

Dr. Venayagamoorthy is a 2004 National Science Foundation CAREER Award recipient, the 2004 IEEE St. Louis Section Outstanding Young Engineer, the 2003 International Neural Network Society (INNS) Young Investigator Award recipient, a 2001 recipient of the IEEE Computational Intelligence Society (CIS) summer research scholarship, and the recipient of five Prize Paper Awards from the IEEE Industry Applications Society (IAS) and the IEEE CIS. He is an Associate Editor of the IEEE TRANSACTIONS ON NEURAL NETWORKS. He is a Senior Member of the South African Institute of Electrical Engineers and a Member of the INNS and the American Society for Engineering Education. He is currently the IEEE St. Louis CIS and IAS Chapter Chairs and the Chair of the Task Force on Intelligent Control Systems and the Secretary of the Intelligent Systems Subcommittee of the IEEE Power Engineering Society. He was the Technical Program Co-Chair of the 2003 International Joint Conference on Neural Networks, Portland, OR, and the 2004 International Conference on Intelligent Sensing and Information Processing, Chennai, India.

Radha Padma Kalyani (S'03) received the B.E. degree in electrical and electronics engineering in 2000 from Andhra University, Visakhapatnam, India, and the M.S. degree in electrical engineering in 2003 from the University of Missouri, Rolla (UMR), where she is currently working toward the Ph.D. degree in electrical engineering.

She is also currently a Research Assistant and Teaching Assistant at UMR. Her research interests include FACTS, power system stability, economic operations of power systems, and artificial intelligence.